

# IS THE HYPERSCALING RELATION VIOLATED BELOW THE UPPER CRITICAL DIMENSION IN SOME PARTICULAR CASES ?

Hung T. Diep<sup>(a)</sup> \* and Van-Thanh Ngo<sup>(b)†</sup>

<sup>(a)</sup> *Laboratoire de Physique Théorique et Modélisation,  
CY Cergy Paris Université, CNRS, UMR 8089  
2 Avenue Adolphe Chauvin,  
95302 Cergy-Pontoise, France*

<sup>(b)</sup> *Institute of Scientific Data and Information,  
Vietnam Academy of Science and Technology (VAST)  
18 Hoang Quoc Viet, Hanoi 10000, Vietnam*

(Dated: July 4, 2025)

In this review, we show our results with new interpretation on the critical exponents of thin films obtained by high-performance multi-histogram Monte Carlo simulations. The film thickness  $N_z$  consists of a few layers up to a dozen of layers in the  $z$  direction. The free boundary condition is applied in this direction while in the  $xy$  plane periodic boundary conditions are used. Large  $xy$  plane sizes are used for finite-size scaling. The Ising model is studied with nearest-neighbor (NN) interaction. When  $N_z = 1$ , namely the two-dimensional (2D) system, we find the critical exponents given by the renormalization group. While, for  $N_z > 1$ , the critical exponents calculated with the high-precision multi-histogram technique show that they deviate slightly but systematically from the 2D values. If we argue that as long as the thickness  $N_z$  is small enough, the correlation length in the  $z$  direction is finite, it does not affect the nature of the phase transition, namely it remains in the 2D universality class. This argument is in contradiction with our numerical results which show a systematic deviation from 2D values. If we use these values of critical exponents in the hyperscaling relation with  $d = 2$ , then the hyperscaling relation is violated. However, if we use the hyperscaling relation and the critical exponents obtained for  $N_z > 1$  to calculate the dimension of the system, we find the system dimension slightly larger than 2. This can be viewed as an "effective" dimension. More discussion is given in the paper. We also show the cross-over between the first- and second-order transition while varying the film thickness in an antiferromagnetic FCC Ising frustrated thin film. In addition, we will show evidence that when a 2D system has two order parameters of different symmetries with a single transition, the critical exponents are new, suggesting a universality class of coupled two-symmetry breakings. In this case, the 2D hyperscaling does not hold. Another case is the 3D Ising model coupled to the lattice vibration: the critical exponents deviate from the 3D Ising ones, the results suggest the violation of the hyperscaling.

**PACS numbers:**

**Keywords: Critical Exponents; Thin Films; Hyperscaling Relations; Effective Dimension;  
Multi-Histogram Monte Carlo Technique.**

## I. INTRODUCTION

The study of phase transitions is one of the most important tasks in theory, in experiments and in computer simulations since the second half of the 20th century. The main reason is that, if we know the characteristics of a phase transition, we can understand the interaction mechanisms lying behind the transition and we can deduce various physical quantities. Therefore, comparisons between theories, experiments and computer simulations are necessary in order to obtain conclusions. While comparison with experiments is always a challenge because real materials may contain ill-controlled elements such as dislocations, defects and impurities, comparisons between theories and simulations are in most cases possible. This is the purpose of the present short review based on our own works in the past years (see our works cited in [1, 2]).

Let us recall that the phase transition was first studied by the mean-field approximation with several improved versions in the 40s (see the textbook [3] where these methods are shown and commented). These were followed by exact-solution methods in two dimensions (2D) such as the Ising model, Potts models and vertex models (see the book by R. Baxter [4]). The break-through in general dimensions come in 1970 with the formulation of the renormalization

---

\* diep@cyu.fr, corresponding author

† nvthanh@vast.vn

group by K. G. Wilson [5, 6] followed by investigations on the finite-size scaling analysis and their validity [7–9]. As known, there are six critical exponents and there are four relations between them. One is called ‘hyperscaling relation’ connected with the space dimension  $d$ . There have been investigations on the progress made on the scaling and hyperscaling relations above the upper critical dimension  $d_u = 4$ . The reader is referred, for example, to Ref.[10] and the review by Young [11] for a recall of the demonstration of these relations (see also the review by Honchar et al. [12]). It should be added that this violation is explained in the framework of Renormalization-Group theory by the existence of a dangerous irrelevant variable [13]. The main question is whether or not the hyperscaling is violated for dimension  $d$  larger than the upper critical dimension  $d_u = 4$ . In the present paper, however, we show that the question of the violation of the hyperscaling is also posed in  $d < 4$  in some specific cases that we will present in this paper. It should be mentioned that Renormalization-Group calculations conclude that the hyperscaling relation should hold for thin films in the case of large- $N$  limit [14]. But in the present paper, we consider thin films of Ising spins ( $N = 1$ ) in section II, so the result of this paper does not apply.

The first case studied in the present paper concerns the critical exponents obtained by using the highly-precise multi-histogram Monte Carlo (MC) technique [15–17] for a thin film of simple cubic structure with Ising spin model. The film surface  $L^2$  ( $xy$  plane) is very large, up to  $L^2 = 160^2$  lattice sites for some cases, with periodic boundary conditions, while the film thickness  $N_z$  goes from one layer (2D) to 13 layers with free boundary conditions. Finite-size scaling (FSS) has been used with varying  $L$  to calculate the critical exponents. These results have been published in Ref. [18] but the aspect of the violation of the hyperscaling relation has not been discussed. In the light of the violation of the hyperscaling relation for  $d \geq d_u$  [10, 11], we revise the interpretation of our results. In addition, we review some other cases that we have investigated.

Except the case  $N_z = 1$ , the question of the dimension of the system naturally arises. For Capehart and Fisher [19], there is a cross-over from 2D to 3D when  $N_z$  is increased. So, how should one use the hyperscaling relation, namely with which dimension? We will discuss this in this paper.

This review is organized as follows. Section II is devoted to the case of thin films mentioned above where the multi-histogram technique is recalled. Section III shows the results of critical exponents obtained with the FSS. Section IV reviews the case of a cross-over between the first- and second-order transitions when the film thickness of a frustrated antiferromagnetic FCC film is decreased. Section V is devoted to some other cases where the hyperscaling relation is violated or seems to be violated. Concluding remarks are given in section VI.

## II. CRITICAL BEHAVIOR OF THIN FILMS

### A. Model

We consider a thin film composing of  $N_z$  layers of  $xy$  square lattices stacking in the  $z$  direction. The  $xy$  plane has the dimension  $L \times L$  where  $L$  is the linear dimension. We use a simple Hamiltonian which consists of Ising spins occupying the lattice sites. The spins interact with each other via an exchange interaction  $J$  between nearest neighbors (NN). We assume  $J$  to be uniform everywhere including between surface spins. The Hamiltonian is written as

$$\mathcal{H} = -J \sum_{i,j} \sigma_i \sigma_j. \quad (1)$$

In the simulations which will be shown below, we take  $N_z$  from 1 to 13 and  $L = 20 - 80$  (for some cases  $L$  is up to 160). Before showing our results, let us summarize the multi-histogram technique in the following.

### B. Multi-histogram Technique

The principle of a single histogram MC method is to record the energy histogram  $H(E)$  collected at a temperature  $T$  as close as possible to the transition temperature obtained from the standard MC simulation. From  $H(E)$  one can calculate thermodynamic quantities using formulas of the canonical distribution. The error depends on how far the chosen temperature is from the transition temperature  $T_c$ . Multi-histogram technique helps overcome this uncertainty. We know that with a finite-size system the maximum of the specific heat  $C_v$  and the maximum of the susceptibility  $\chi$  do not occur at the same temperature. In the multi-histogram technique, we take another temperature close to the maximum of  $C_v$  and the maximum of  $\chi$  to calculate by histogram technique the new temperatures of the maxima of  $C_v$  and  $\chi$ . We repeat again this procedure for 8 temperatures: such an iteration procedure improves the positions of the maxima of  $C_v$  and  $\chi$  at the system size  $(L, N_z)$ . The reader is referred to Refs. [16, 17] for more technical

details. Note that, as in the single histogram technique, thermal physical quantities are calculated as continuous functions of  $T$  which allow for the precise determination of the peak positions and the peak heights of  $C_v$  and  $\chi$  for a given system size. This permits making the finite-size scaling with precision. In addition, since we take many temperatures in the transition region, the results obtained by multi-histogram method are valid for a wider range of temperature, unlike a single histogram technique with the results valid only in a very small temperature region, typically  $[T - T_c(\infty)]/T_c(\infty) \simeq \pm 1\%$ .

The multiple histogram technique is known to reproduce with very high accuracy the critical exponents of second order phase transitions.[15–17] The overall probability distribution[16] at temperature  $T$  obtained from  $n$  independent simulations, each with  $N_j$  configurations, is given by

$$P(E, T) = \frac{\sum_{i=1}^n H_i(E) \exp[E/k_B T]}{\sum_{j=1}^n N_j \exp[E/k_B T_j - f_j]}, \quad (2)$$

where

$$\exp[f_i] = \sum_E P(E, T_i). \quad (3)$$

The thermal average of a physical quantity  $A$  is then calculated by

$$\langle A(T) \rangle = \sum_E A P(E, T) / z(T), \quad (4)$$

in which

$$z(T) = \sum_E P(E, T). \quad (5)$$

Thermal averages of physical quantities are thus calculated as continuous functions of  $T$ , now the results should be valid over a much wider range of temperature than for any single histogram. In practice, we use first the standard MC simulations to localize for each size the transition temperatures  $T_0^E(L)$  for specific heat and  $T_0^m(L)$  for susceptibility. The equilibrating time is from 200000 to 400000 MC steps/spin and the averaging time is from 500000 to 1000000 MC steps/spin. Next, we make histograms at 8 different temperatures  $T_j(L)$  around the transition temperatures  $T_0^{E,m}(L)$  with 2 millions MC steps/spin, after discarding 1 millions MC steps/spin for equilibrating. Finally, we make again histograms at 8 different temperatures around the new transition temperatures  $T_0^{E,m}(L)$  with  $2 \times 10^6$  and  $4 \times 10^6$  MC steps/spin for equilibrating and averaging time, respectively. Such an iteration procedure gives extremely good results for systems studied so far. Errors shown in the following have been estimated using statistical errors, which are very small thanks to our multiple histogram procedure, and fitting errors given by fitting software.

In MC simulations, we calculate the thermal averages of

- the magnetization  $\langle M \rangle$

$$\langle M \rangle = \frac{1}{L^2 N_z} \langle \sum_i \sigma_i \rangle, \quad (6)$$

- the total energy  $\langle E \rangle$ ,

$$\langle E \rangle = \langle \mathcal{H} \rangle, \quad (7)$$

- the heat capacity  $C_v$ ,

$$C_v = \frac{1}{k_B T^2} (\langle E^2 \rangle - \langle E \rangle^2), \quad (8)$$

- the susceptibility  $\chi$ ,

$$\chi = \frac{1}{k_B T} (\langle M^2 \rangle - \langle M \rangle^2), \quad (9)$$

- the Binder energy cumulant  $U$ ,

$$U = 1 - \frac{\langle E^4 \rangle}{3 \langle E^2 \rangle^2}, \quad (10)$$

$-n^{\text{th}}$  order cumulant of the order parameter  $V_n$  for  $n = 1$  and 2:

$$V_n = \frac{\partial \ln M^n}{\partial(1/k_B T)} = \langle E \rangle - \frac{\langle M^n E \rangle}{\langle M^n \rangle}. \quad (11)$$

Note that if we scale with  $L$ , we have the following relations, since  $N_z$  is fixed [11, 16, 20]:

$$V_1^{\max} \propto L^{1/\nu}, \quad V_2^{\max} \propto L^{1/\nu}, \quad (12)$$

$$C_v^{\max} = C_0 + C_1 L^{\alpha/\nu} \quad (13)$$

and

$$\chi^{\max} \propto L^{\gamma/\nu}, \quad (14)$$

at their respective 'transition' temperatures  $T_c(L)$ , and

$$U = U[T_c(\infty)] + AL^{-\alpha/\nu}, \quad (15)$$

$$M_{T_c(\infty)} \propto L^{-\beta/\nu}, \quad (16)$$

and

$$T_c(L) = T_c(L = \infty) + C_A L^{-1/\nu}. \quad (17)$$

In the above relations,  $A$ ,  $C_0$ ,  $C_1$  and  $C_A$  are constants. The exponent  $\nu$  can be calculated by Eqs. (12). For  $L$  large enough,  $V_1^{\max}$  and  $V_2^{\max}$  should give the same  $\nu$  as seen below. Then, from Eq. (17) we estimate  $T_c(L = \infty)$ . Using this, we calculate  $\alpha$  and  $\beta$  from Eqs. (15) and (16). We will check the Rushbrooke inequality  $\alpha + 2\beta + \gamma \geq 2$  and the hyperscaling relation  $d\nu = 2 - \alpha$  in the following.

To ensure that Eqs. (12)-(17) are used for  $L$  large enough, one uses the following corrections to scaling of the form

$$\chi^{\max} = B_1 L^{\gamma/\nu} (1 + B_2 L^{-\omega}), \quad (18)$$

$$V_n^{\max} = D_1 L^{1/\nu} (1 + D_2 L^{-\omega}), \quad (19)$$

$B_1$ ,  $B_2$ ,  $D_1$  and  $D_2$  being constants and  $\omega$  a correction exponent.[21] Normally, if  $L$  is large enough, the corrections are very small. With today's computer memory capacity, large  $L$  is often used as seen below. The scaling corrections are thus extremely small, they do not therefore alter the results using Eqs. (12)-(17).

### III. RESULTS

Most of the results shown below have been published by us in [18]. However, in light of the new interpretation on the violation of the hyperscaling relation, we review them here to show that there is a possibility that the hyperscaling relation  $d\nu = 2 - \alpha$  is violated below  $d_u$ : as mentioned in the Introduction, in the case of thin films where the thickness is finite and small, the hyperscaling relation is satisfied only when  $d$  has a value between 2 and 3. This non-integer dimension is called by Capohart and Fisher [19] "cross-over dimension". To our knowledge,  $d$  in the hyperscaling relation is the space dimension, it is 2, 3, ... (integer), it cannot be between 2 and 3. We are convinced that the hyperscaling relation may not be valid in the case of thin films shown below and in other particular cases shown in section V.

First, we show the layer magnetizations and their corresponding susceptibilities of the first three layers in the case where  $N_z = 5$ ,  $L = 24$  in Fig. 1. The layer susceptibilities have their peaks at the same temperature, indicating a single transition. We note that the magnetization is lowest at the surface and increases while going to the interior. This is known a long time ago by the Green's function method [3, 22, 23] and by more recent works on thin films with competing interactions [24] and films with Dzyaloshinskii-Moriya interaction [25, 26]. Physically, the surface spins have smaller local field due to the lack of neighbors, so thermal fluctuations will reduce more easily the surface magnetization with respect to the interior ones. We plot in Fig. 2 the total magnetization and the total susceptibility. The latter shows only one peak, signature of a single transition. This justifies the study shown below on the criticality of the film transition.

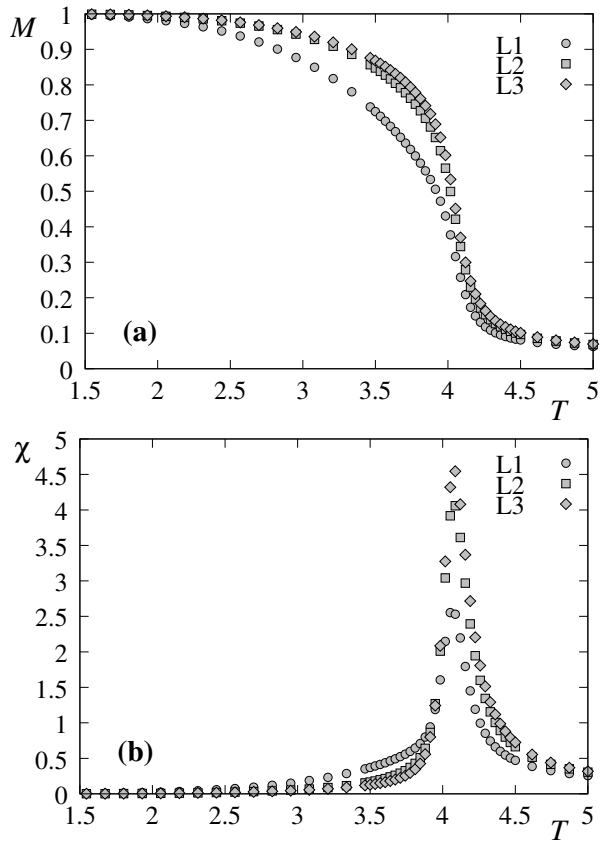


FIG. 1: (a) Layer magnetizations of layer 1 (denoted by  $L_1$ ), layer 2 (denoted by  $L_2$ ) and layer 3 (denoted by  $L_3$ ), (b) Layer susceptibilities, as functions of  $T$  with  $N_z = 5$  and  $L = 24$ .

### A. Finite size scaling

Let us show our finite-size scaling (FSS) with  $L$  varying from 20 to 80. For  $N_z = 3$  we use  $L$  up to 160 to evaluate the corrections to scaling. The technical details are described in the subsection IIB above. Note that the multi-histograms at 8 temperatures in the critical region have been performed iteratively many times. Such an iteration procedure gives extremely good results. Errors shown in the following have been estimated using statistical errors, which are very small thanks to our multiple histogram procedure, and fitting errors given by fitting software. Note that the errors are at the 3rd digit as seen in Table I, they are smaller than the size of the data points shown in the figures.

### B. Critical exponents obtained with finite-size scaling

We show first the peak height of the susceptibility and the maximum of  $V_1$  as functions of  $T$  for varying  $L$  from 20 to 80 in Fig. 3.

Note that the results shown below are obtained using  $T_c(L = \infty, N_z)$  as described earlier below Eq. (17). We show in Fig. 4  $V_1^{max}$  versus  $L$  in the  $\ln - \ln$  scale for  $N_z = 1, 3, \dots, 13$ . The slope of a given straight line gives  $1/\nu$  of the corresponding  $N_z$ . Exponent  $\nu$  obtained from Fig. 4 is shown as a function of  $N_z$  in Fig. 5

To show the precision of our method, we give here the results of  $N_z = 1$ . For  $N_z = 1$ , we have  $1/\nu = 1.0010 \pm 0.0028$  which yields  $\nu = 0.9990 \pm 0.0031$  and  $\gamma/\nu = 1.7537 \pm 0.0034$  and  $\gamma = 1.7520 \pm 0.0062$ . These results are in excellent agreement with the exact results  $\nu_{2D} = 1$  and  $\gamma_{2D} = 1.75$ . The very high precision of our method is thus verified in the rather modest range of the system sizes  $L = 20 - 80$  used in the present work. Note that the result of Ref.[27] gave  $\nu = 0.96 \pm 0.05$  for  $N_z = 1$  which is very far from the exact value. The results of  $\gamma/\nu$  are shown in Figs. 6 and 7. The results of  $\alpha/\nu$  are shown in Fig. 8. These critical exponents are, although close to those of 2D, show a systematic deviation from the 2D case with increasing  $N_z$ .

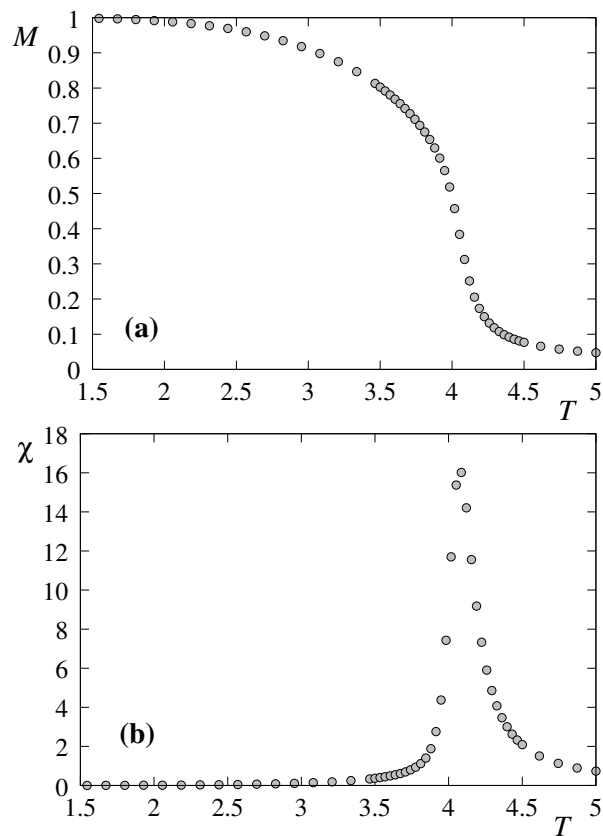


FIG. 2: (a) Total magnetization, (b) Total susceptibility, versus  $T$  with  $N_z = 5$  and  $L = 24$ .

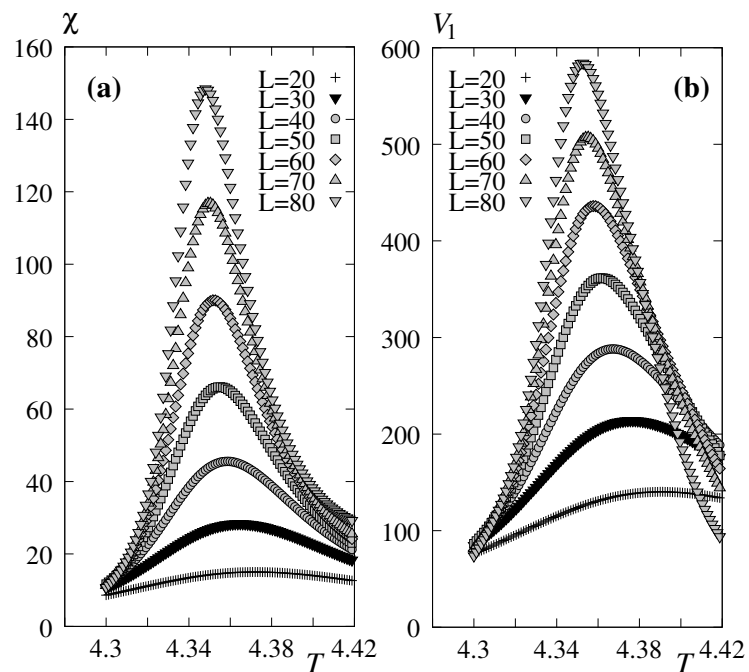


FIG. 3: (a) Susceptibility and (b)  $V_1$ , as functions of  $T$  for  $L = 20, 30, \dots, 80$  with  $N_z = 11$ , obtained by multiple histogram technique. Note the strong dependence of the peak height on  $L$ .

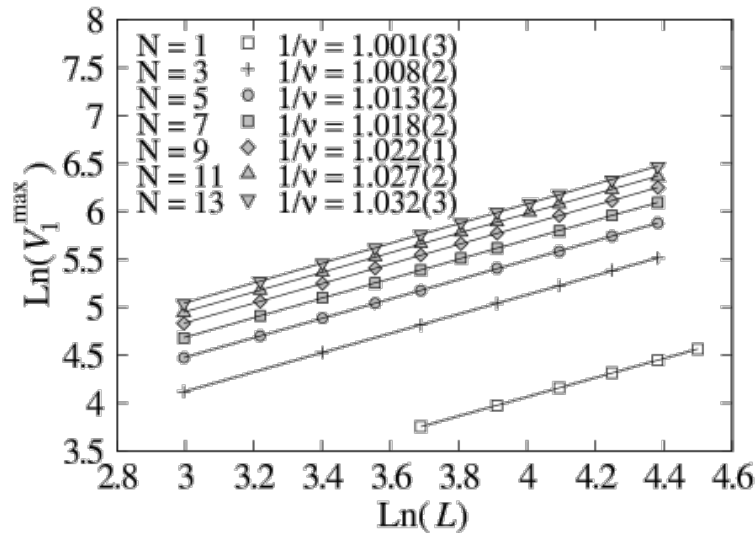


FIG. 4: Maximum of  $V_1$  versus  $L$  in the  $\ln - \ln$  scale for various  $N_z$ . The slopes give  $1/\nu$  [see Eq. (12)]. These values are indicated on the figure.

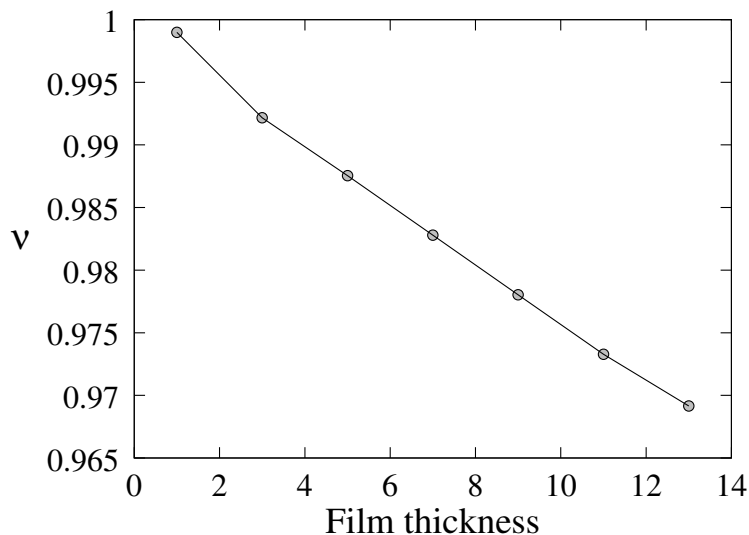


FIG. 5: Exponent  $\nu$  versus  $N_z$ . Note that  $\nu(2D) = 1$  and  $\nu(3D) = 0.62997$ .

### C. Corrections to scaling

Let us touch upon the question of corrections to scaling mentioned earlier. We show now that the corrections to scaling are very small. We consider here the effects of larger  $L$  and of the correction to scaling for  $N_z = 1, 3, \dots, 13$ . The results indicate that larger  $L$  does not change the results shown above. Figure 9(a) displays the maximum of  $V_1$  as a function of  $L$  up to 160. Using Eq. (12), i.e. without correction to scaling, we obtain  $1/\nu = 1.009 \pm 0.001$  which is to be compared to  $1/\nu = 1.008 \pm 0.002$  using  $L$  up to 80. The change is therefore insignificant because it is at the third decimal i. e. at the error level. The same is observed for  $\gamma/\nu$  as shown in Fig. 9(b):  $\gamma/\nu = 1.752 \pm 0.002$  using  $L$  up to 160 instead of  $\gamma/\nu = 1.751 \pm 0.002$  using  $L$  up to 80.

Now, let us allow for correction to scaling, i. e. we use Eq.(18) instead of Eq. (14) for fitting. We obtain the following values:  $\gamma/\nu = 1.751 \pm 0.002$ ,  $B_1 = 0.05676$ ,  $B_2 = 1.57554$ ,  $\omega = 3.26618$  if we use  $L = 70$  to 160 (see Fig. 10). The value of  $\gamma/\nu$  in the case of no scaling correction is  $1.752 \pm 0.002$ . Therefore, we can conclude that this correction is insignificant. The large value of  $\omega$  explains the smallness of the correction.

For  $\beta$ , using Eq. (16) we calculate  $\beta/\nu$  for each thickness  $N_z$ . The results are precise. For example for  $N_z=1$ , we

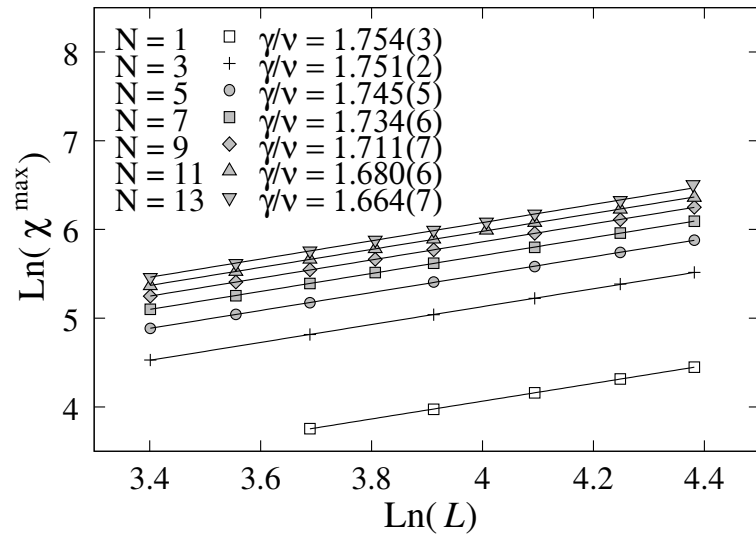


FIG. 6: Maximum of susceptibility versus  $L$  in the  $\ln - \ln$  scale. The slopes give  $\gamma/\nu$  indicated on the figure.

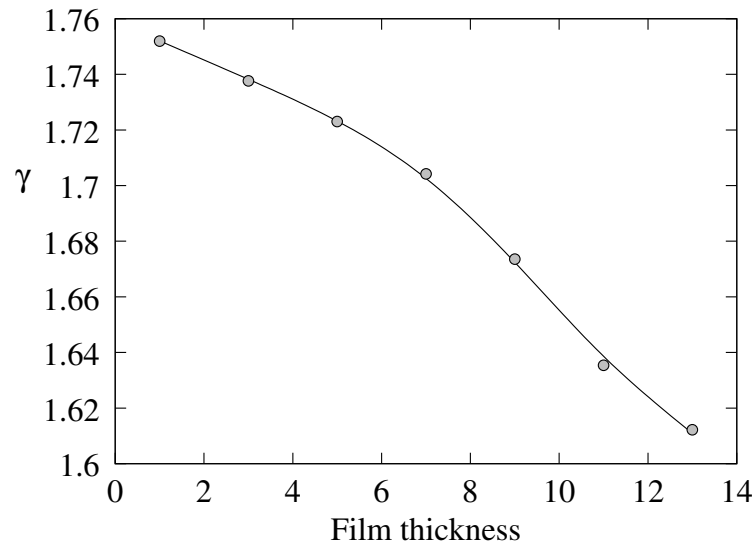


FIG. 7: Exponent  $\gamma$  versus  $N_z$ . Note that  $\gamma(2D) = 1.75$  and  $\gamma(3D) = 1.23707$ .

obtained  $\beta/\nu = 0.1268 \pm 0.0022$  which yields  $\beta = 0.1266 \pm 0.0049$  which is in agreement within errors with the exact result  $\beta = 1.25$ . We show in Fig. 11 the exponent  $\beta$  versus  $N_z$ .

#### D. Summary of our results

We summarize our results in Table I. Note that if we use  $\nu$  and  $\alpha$  for a given  $N_z$ , except the case  $N_z = 1 (d = 2)$ , the hyperscaling relation  $d\nu = 2 - \alpha$  is violated if  $d = 2$ . This relation is obeyed if the dimension is replaced by an "effective dimension"  $d_{\text{eff}}$  listed in Table I which is a little bit larger than 2. This means that the 2D critical behavior dominates in thin films as expected ( $d_{\text{eff}}$  varies from 2 to 2.0613 for  $N_z = 1$  to 13). The last column shows the critical temperature at  $L = \infty$  obtained by using Eq. (17).

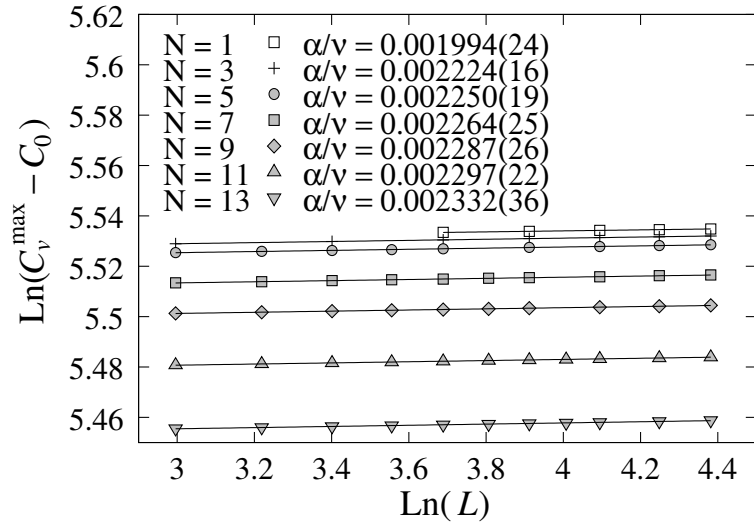


FIG. 8:  $\ln(C_v^{\max} - C_0)$  versus  $\ln L$  for  $N_z = 1, 3, 5, \dots, 13$ . The slope gives  $\alpha/\nu$  (see Eq. 13) indicated on the figure. Note that  $\alpha/\nu(2D) = 0$  and  $\alpha/\nu(3D) = 0.110087/0.62997 = 0.174749$ .

$N_z$	$\nu$	$\gamma$	$\alpha$	$\beta$	$d_{\text{eff}}$	$T_c(L = \infty, N_z)$
1	$0.9990 \pm 0.0028$	$1.7520 \pm 0.0062$	$0.00199 \pm 0.00279$	$0.1266 \pm 0.0049$	$2.0000 \pm 0.0028$	$2.2699 \pm 0.0005$
3	$0.9922 \pm 0.0019$	$1.7377 \pm 0.0035$	$0.00222 \pm 0.00192$	$0.1452 \pm 0.0040$	$2.0135 \pm 0.0019$	$3.6365 \pm 0.0024$
5	$0.9876 \pm 0.0023$	$1.7230 \pm 0.0069$	$0.00222 \pm 0.00234$	$0.1639 \pm 0.0051$	$2.0230 \pm 0.0023$	$4.0234 \pm 0.0028$
7	$0.9828 \pm 0.0024$	$1.7042 \pm 0.0087$	$0.00223 \pm 0.00238$	$0.1798 \pm 0.0069$	$2.0328 \pm 0.0024$	$4.1939 \pm 0.0032$
9	$0.9780 \pm 0.0016$	$1.6736 \pm 0.0084$	$0.00224 \pm 0.00161$	$0.1904 \pm 0.0071$	$2.0426 \pm 0.0016$	$4.2859 \pm 0.0022$
11	$0.9733 \pm 0.0025$	$1.6354 \pm 0.0083$	$0.00224 \pm 0.00256$	$0.1995 \pm 0.0088$	$2.0526 \pm 0.0026$	$4.3418 \pm 0.0032$
13	$0.9692 \pm 0.0026$	$1.6122 \pm 0.0102$	$0.00226 \pm 0.00268$	$0.2059 \pm 0.0092$	$2.0613 \pm 0.0027$	$4.3792 \pm 0.0034$

TABLE I: Critical exponents obtained by multi-histogram technique. The effective dimension and critical temperature  $T_c(L = \infty, N_z)$  are listed in the last two columns. See text for the definition of the effective dimension  $d_{\text{eff}}$ .

### E. Discussion

Let us show in Fig. 12 the effective dimension versus  $N_z$ . As seen, though  $d_{\text{eff}}$  deviates systematically from  $d = 2$ , its values are however very close to 2. This means that the 2D character is dominant even at  $N_z = 13$ .

As mentioned above,  $d_{\text{eff}}$  is very close to 2. However,  $T_c(L = \infty, N_z)$  increases very fast to reach a value close to  $T_c$  of the 3D Ising model ( $\simeq 4.51$ ) at  $N_z = 13$ . This is an interesting point. In Ref. [19] Capehart and Fisher define the critical-point shift as

$$\varepsilon(N_z) = [T_c(L = \infty, N_z) - T_c(3D)] / T_c(3D). \quad (20)$$

They showed that

$$\varepsilon(N_z) \approx \frac{b}{N_z^{1/\nu}} [1 + a/N_z], \quad (21)$$

where  $\nu = 0.6289$  (3D value). Using  $T_c(3D) = 4.51$ , we fit the above formula with  $T_c(L = \infty, N_z)$  taken from Table I, we obtain  $a = -1.37572$  and  $b = -1.92629$ . Our results and the fitted curve are shown in Fig. 13. Note that the correction factor  $[1 + a/N_z]$  is necessary to obtain a good fit for small  $N_z$ . The prediction of Capehart and Fisher is verified by our result.

If the cross-over dimension raised by Capehart and Fisher [19] is identified with the effective dimension between 2 and 3, then the hyperscaling relation involving the space dimension  $d$  cannot be satisfied in the case of thin films. Let us take the case  $N_z = 13$ , we have  $d\nu = 2 \times 0.9692 = 1.9384$ , while  $2 - \alpha = 2 - 0.00226 = 1.99774$  far from the  $d\nu$  value. The hyperscaling relation is thus violated.

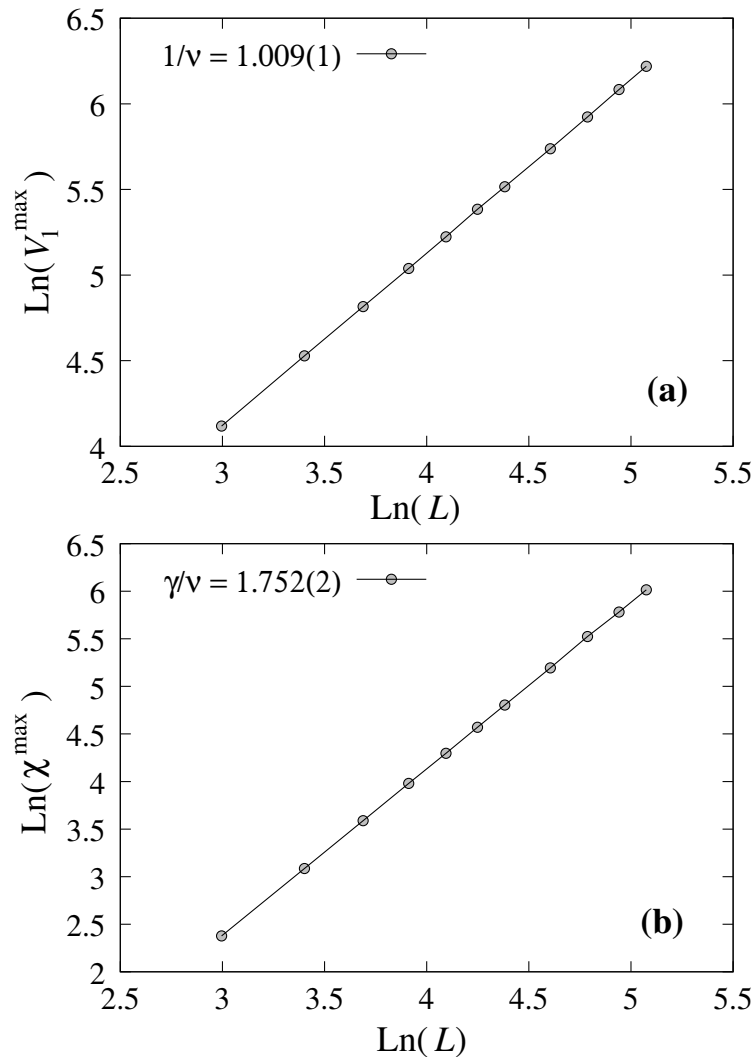


FIG. 9: (a)  $V_1^{\max}$  and (b)  $\chi^{\max}$  vs  $L$  up to 160 with  $N_z = 3$ .

We show now that the free boundary condition in the  $z$  direction gives the same result, within errors, as the periodic boundary condition (PBC), as far as the critical exponents are concerned. This is shown in Figs. 14 and 15.

We would like to emphasize that the Rushbrooke inequality  $\alpha + 2\beta + \gamma \geq 2$  is verified within errors as an equality for each  $N_z$  as seen in Table I.

#### IV. CROSS-OVER FROM FIRST- TO SECOND-ORDER TRANSITION WITH VARYING FILM THICKNESS

In this section, we show that the film thickness can alter the nature of the transition. We cite here our work on the cross-over between the first- and second-order transition when the film thickness of a fully frustrated FCC antiferromagnet with Ising spins is decreased to  $\leq 4$  layers (two FCC cells). We used the highly efficient Wang-Landau method [29–35] to detect the thickness where the first-order transition becomes a second-order one.

Figure 16 shows the strong first-order character of the transition with an energy discontinuity in the bulk case.

In the case of a thin film composed of 8 layers ( $N_z=4$  FCC cells in the  $z$  direction), the first-order character remains as shown in Fig. 17 with a double-peak structure.

When we decrease the film thickness, the latent heat goes to zero at 4 layers (i. e.  $N_z = 2$ ) as shown in Fig. 18.

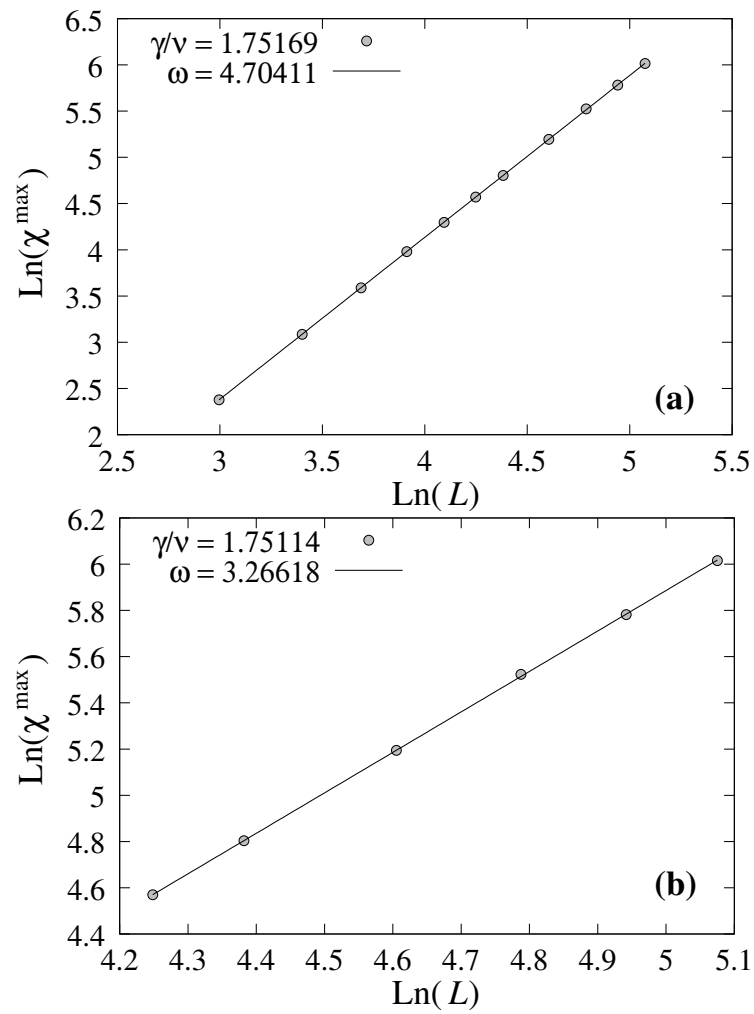


FIG. 10:  $\chi^{\max}$  vs  $L$  (a) from 20 up to 160 (b) from 70 up to 160, for  $N_z = 3$ .

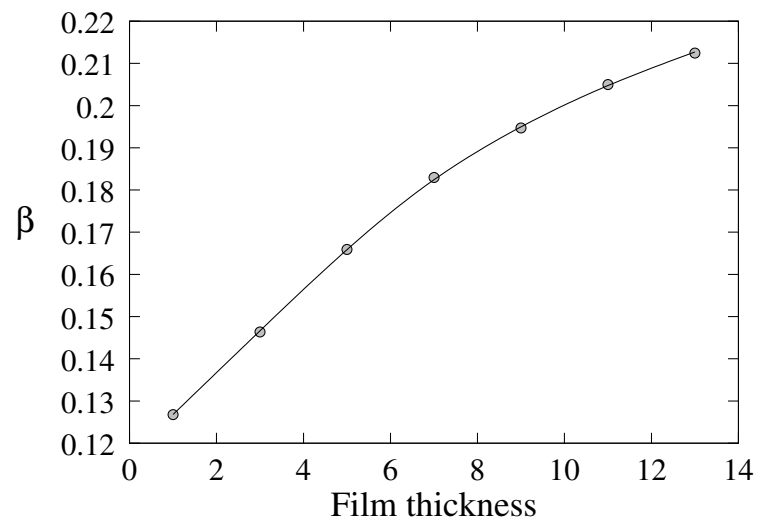


FIG. 11: Exponent  $\beta$  as a function of the film thickness.

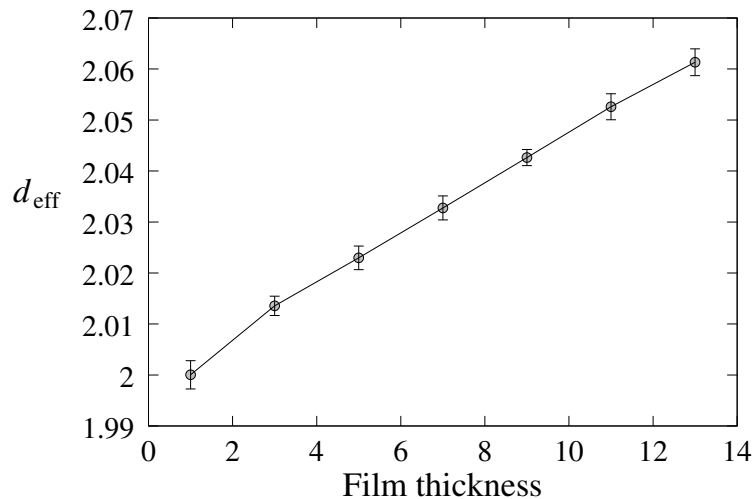


FIG. 12: Effective dimension  $d_{\text{eff}}$  of thin film defined by  $d_{\text{eff}}\nu = 2 - \alpha$ , as a function of thickness. See text for comments.

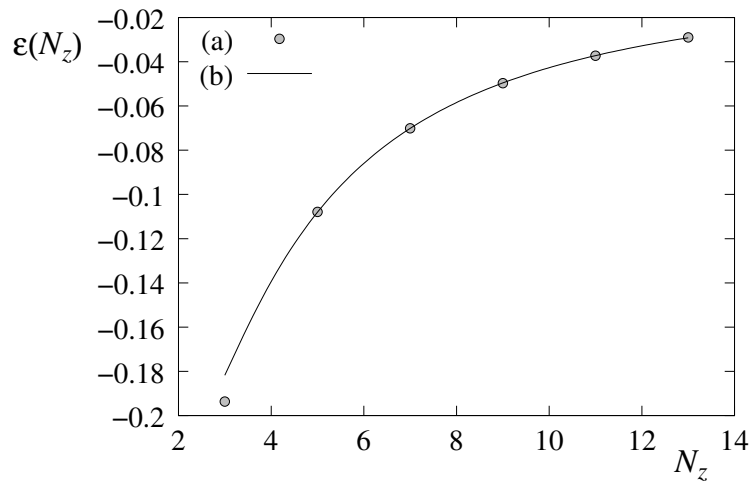


FIG. 13: Critical temperature at infinite  $L$ ,  $T_c(L = \infty, N_z)$ , versus  $N_z$ . MC results are shown by points, continuous line is the prediction of Capehart and Fisher, Eq. (21). The agreement is excellent.

We have fitted  $\Delta E$  with the following function

$$\Delta E = A - \frac{B}{N_z^{d-1}} \left[ 1 + \frac{C}{N_z} \right], \quad (22)$$

where  $d = 3$  is the space dimension,  $A = 0.3370$ ,  $B = 3.7068$ ,  $C = -0.8817$ . The second term in the brackets corresponds to a size correction. As seen in Fig. 18, the latent heat vanishes at a thickness  $L_z = 2N_z = 4$ . This is verified by our simulations for a 4-layer film: the transition has a continuous energy across the transition region, even when  $L = 150$ .

The energy versus  $T$  for  $L_z = 4$  is shown in Fig. 19.

As seen in Fig. 20, there are two close transitions: transition of the surface layers at  $z = 0$  and  $z = 3/2$ , and that of the beneath layers at  $z = 1/2$  and  $z = 1$  (the lattice constant is taken to be 1).

The surface layer has larger magnetization than that of the second layer unlike the non-frustrated case shown in the previous section. One can explain this by noting that due to the lack of neighbors, surface spins are less frustrated than the interior spins, making them more stable than the interior spins. This has been found at the surface of the frustrated helimagnetic film [24]. In order to find the nature of these transitions, using the Wang-Landau technique we study the finite-size effects which are shown in in Figs. 21 and 22. The first peak at  $T_1 \simeq 1.927$  corresponds to the vanishing of the second-layer magnetization, it does not depend on the lattice size, while the second peak at

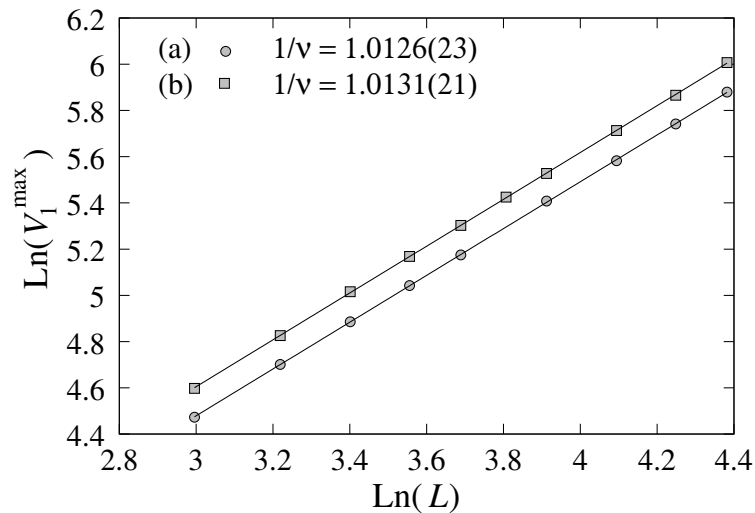


FIG. 14: Maximum of  $V_1$  versus  $L$  in the  $\ln - \ln$  scale for  $N_z = 5$ : (a) without PBC in  $z$  direction (b) with PBC in  $z$  direction. The slopes are indicated on the figure.

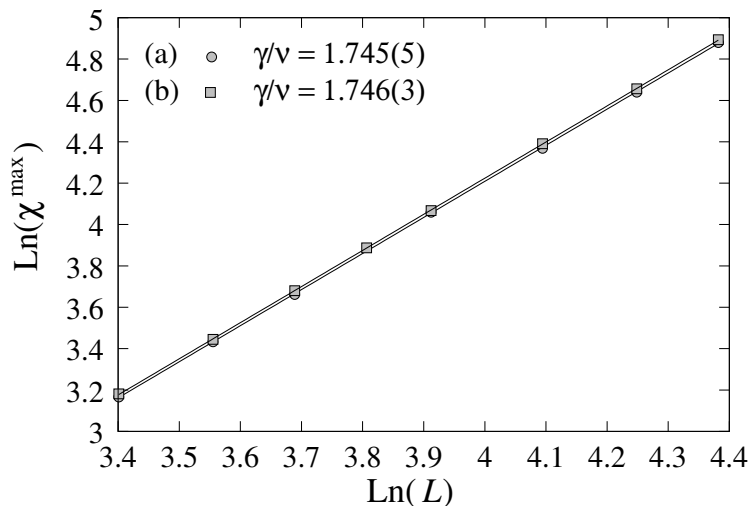


FIG. 15:  $\chi^{\max}$  versus  $L$  in the  $\ln - \ln$  scale for  $N_z = 5$  (a) without PBC in  $z$  direction (b) with PBC in  $z$  direction. The data points of two cases are not distinguishable in the figure scale. The slopes are indicated on the figure.

$T_2 \simeq 1.959$ , corresponding to the disordering of the two surface layers, it depends on  $L$ . The histograms shown in Fig. 23 are taken at and near the transition temperatures show a Gaussian distribution indicating a non first-order transition.

The fact that the peak at  $T_1$  of the specific heat does not depend on  $L$  suggests two scenarios: i)  $T_1$  does not correspond to a transition, ii)  $T_1$  is a Kosterlitz-Thouless transition. We are interested here in the size-dependent transition at  $T_2$ . Using the multi-histogram technique, we have obtained  $\nu = 0.887 \pm 0.009$  and  $\gamma = 1.542 \pm 0.005$  for the case of a 4-layer film (see Figs. 24 and 25). These values do not correspond neither to 2D nor 3D Ising models  $\nu(2D) = 1$ ,  $\gamma(2D) = 1.75$ ,  $\nu(3D) = 0.63$ ,  $\gamma(3D) = 1.241$ . We can interpret this as a dimension cross-over between 2D and 3D. Note that the values we have obtained  $\nu = 0.887 \pm 0.009$  and  $\gamma = 1.542 \pm 0.005$  belong to a new, unknown universality class. At the time of our work [28], we relied on the hyperscaling relation with  $d = 2$  to deduce critical exponent  $\alpha$  and using the Rushbrooke equality to calculate  $\beta$ . However, in view of a possible violation of the hyperscaling when  $d$  is not the space dimension, we cannot conclude without a direct calculation of  $\alpha$  as we have done in the previous section.

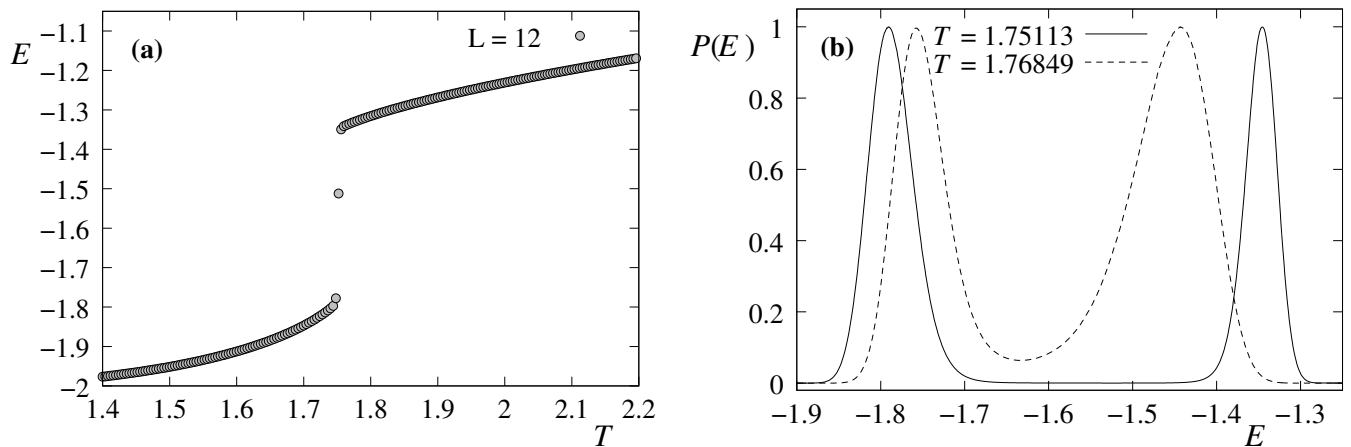


FIG. 16: (a) Energy of the bulk case vs  $T$  for  $L \times L \times L = 12^3$  FCC cells, i. e. the number of spins is  $4L^3$ ; (b) Energy histogram with periodic boundary conditions in all three directions (continuous line) and without PBC (dotted line) in  $z$  direction. The histogram was recorded at the transition temperature  $T_c$  for each case (indicated on the figure).

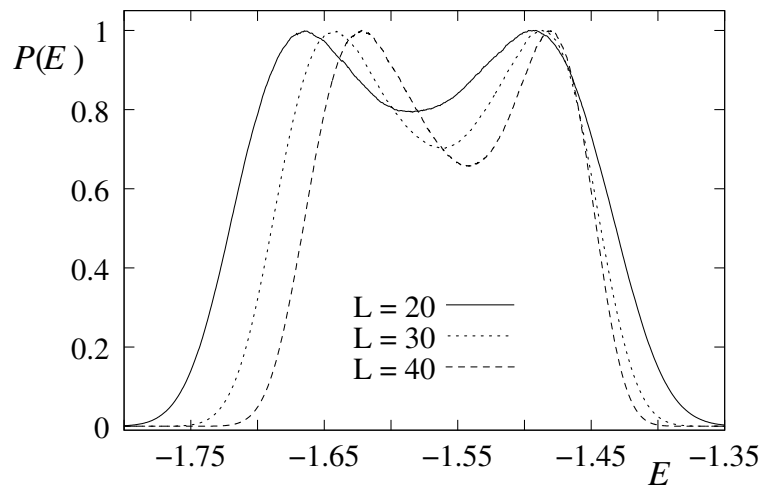


FIG. 17: Energy histogram for  $L = 20, 30, 40$  with film thickness of 8 atomic layers at  $T = 1.8218, 1.8223, 1.8227$ , respectively.

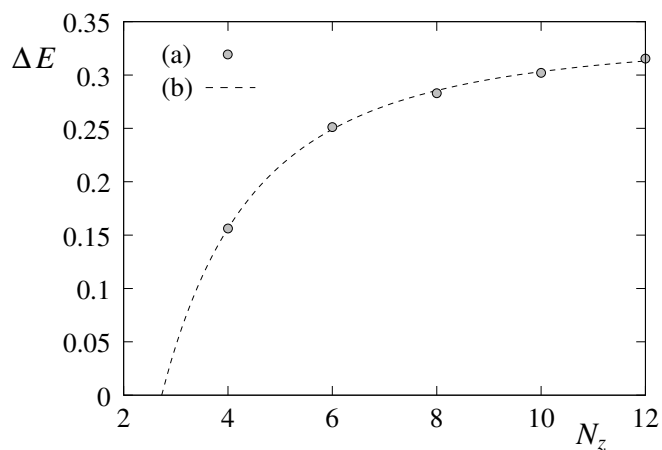


FIG. 18: The latent heat  $\Delta E$  as a function of thickness  $L_z = 2N_z$  (points are MC results). The latent heat goes to zero at  $N_z = 2$ , i.e. at  $L_z = 4$  atomic layers. The continuous line is the fitted function Eq. (22).

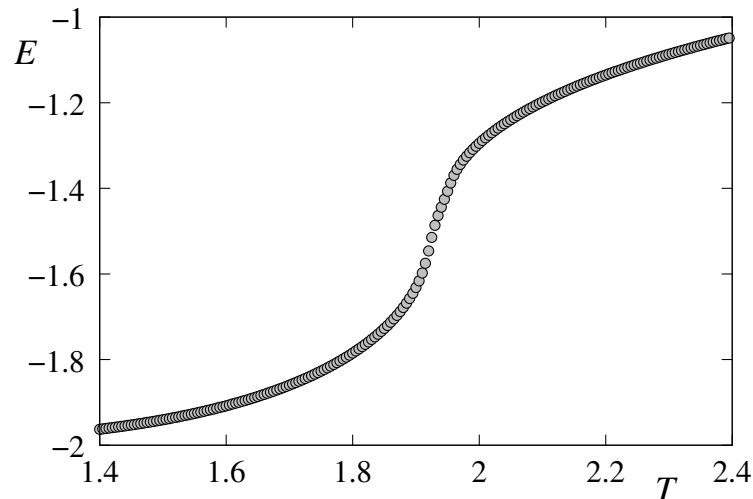


FIG. 19: Energy versus temperature  $T$  for  $L = 120$  for a 4-layer film.

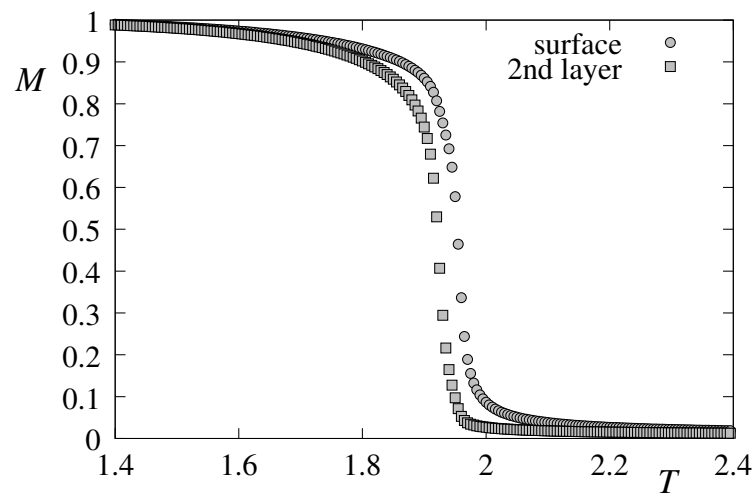


FIG. 20: Layer magnetizations for  $L = 120$  with a 4-layer film: the higher (lower) curve is the surface (beneath) layer magnetization.

## V. OTHER CASES VIOLATING THE HYPERSCALING RELATION ?

There are cases where the systems have an additional degree of freedom distinct from the order parameter. This is the case of XY spins with a chirality symmetry: while the chiral symmetry can be mapped onto an Ising-like symmetry, the continuous nature of XY spins affects the criticality of the Ising symmetry breaking. Another case is a system of Ising spins in which each spin moves around its lattice site, a kind of magneto-elastic coupling. These two cases have been previously studied [36–38]. We briefly review these results below under the view angle of new universality class and the violation or not of the hyperscaling relation below  $d_u = 4$ .

### A. Fully Frustrated XY Square Lattice

The fully frustrated with XY spins on the square lattice has been intensively studied [36, 39–46]. The lattice with the ground-state (GS) spin configuration is shown in Fig. 26 (see [39]) where the angles between spins linked by a ferromagnetic (antiferromagnetic) bond is  $\pi/4$  ( $3\pi/4$ ) with right and left chiralities. This GS is equivalent to an Ising model on an antiferromagnetic square lattice. When  $T$  increases, one expects a transition of the Ising type. However,

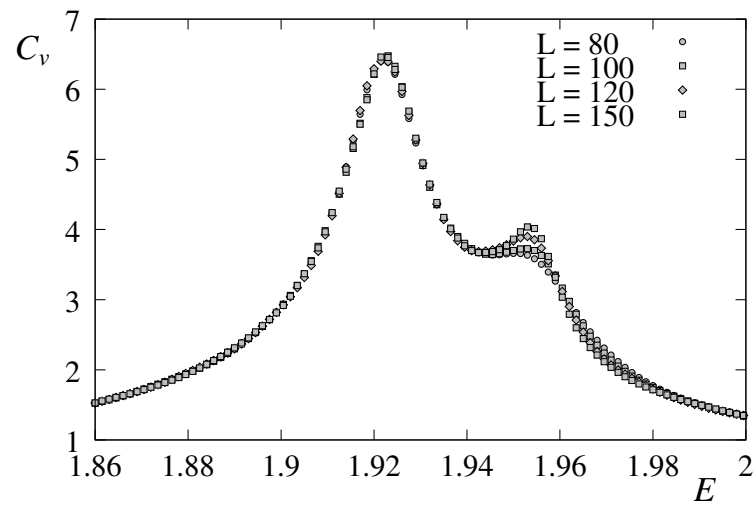


FIG. 21: Specific heat are shown for various linear  $xy$  plane sizes  $L$  versus  $T$  for a 4-layer film.

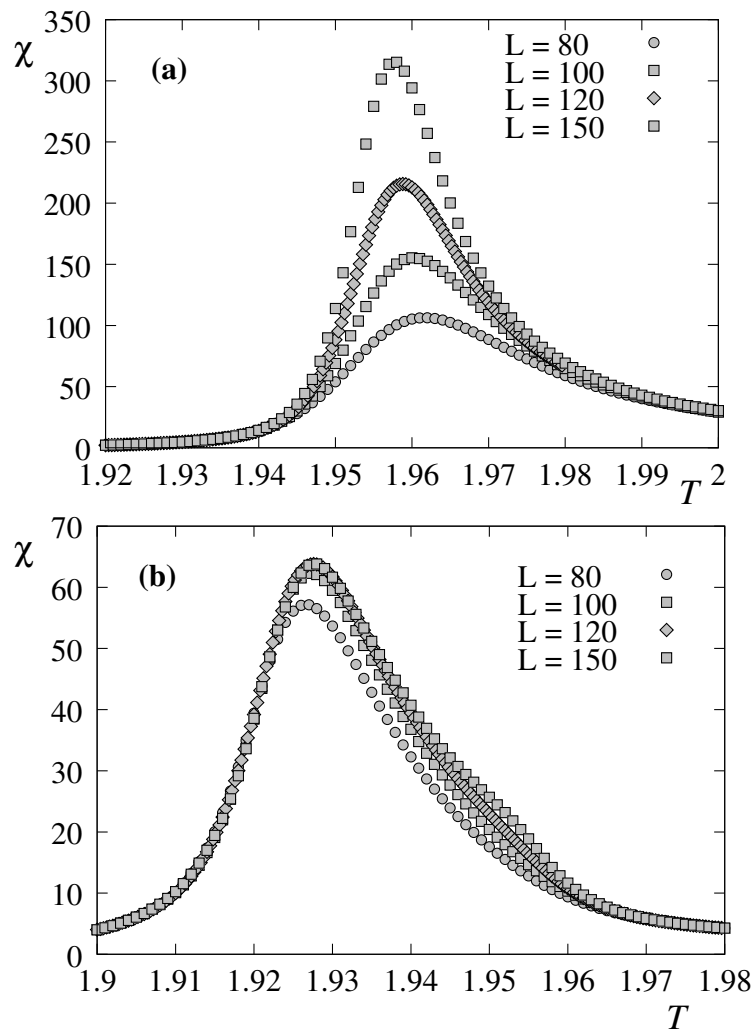


FIG. 22: Susceptibilities of the first layer (a) and the second layer (b) are shown for various sizes  $L$ , versus  $T$  in a 4-layer film.

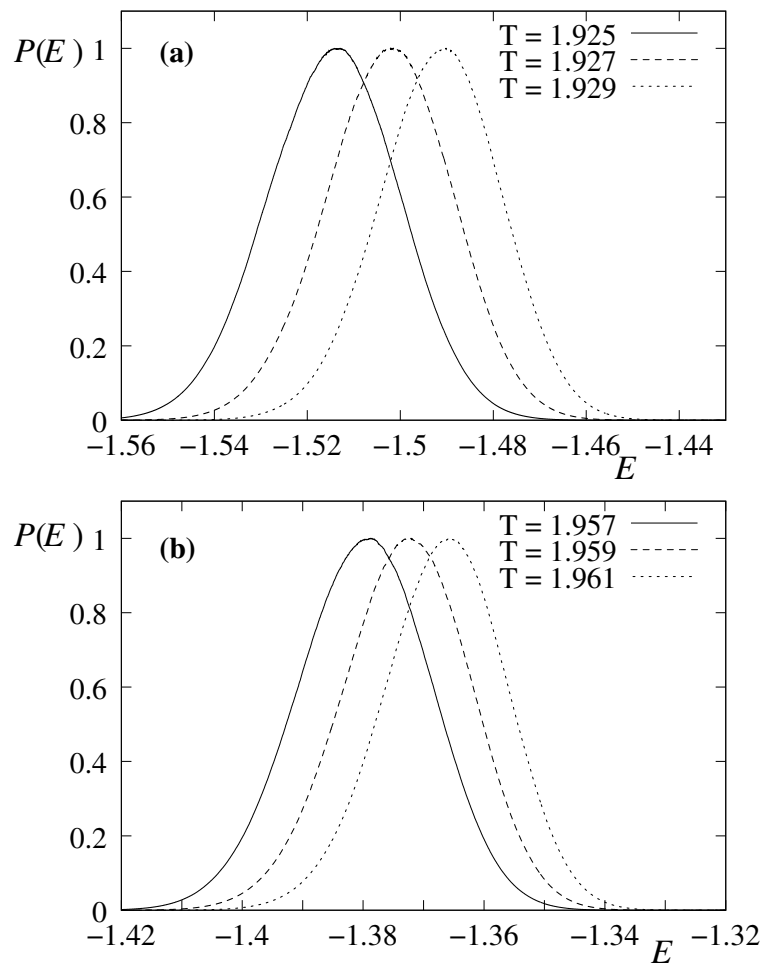


FIG. 23: Energy histograms recorded at temperatures (indicated on the figure) corresponding to the the first (a) and second (b) peaks observed in the specific heat, for  $L = 120$  with 4-layer film thickness  $L_z = 4$ .

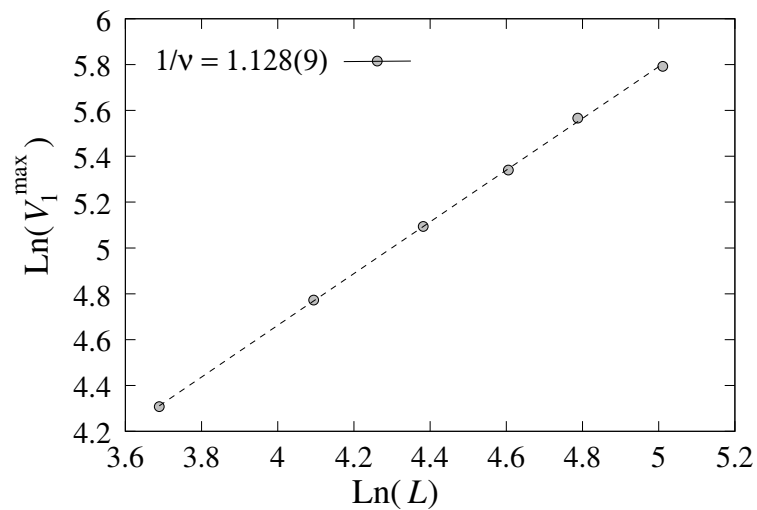


FIG. 24: The maximum value of  $V_1$  as a function of  $L$  in the  $\ln - \ln$  scale. The slope of this straight line gives  $1/\nu$ . The value of  $\nu$  is  $\nu = 0.887 \pm 0.009$ .

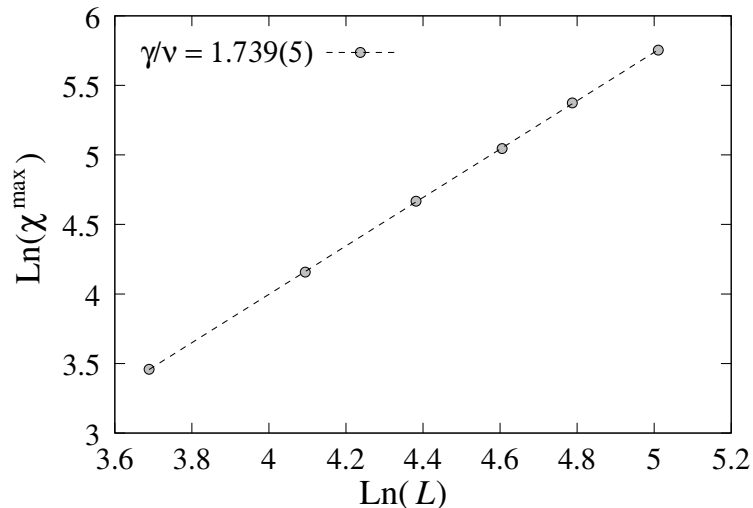


FIG. 25: The maximum of the susceptibility  $\chi^{\max}$  as a function of  $L$  in the  $\ln - \ln$  scale. The slope of this straight line gives  $\gamma/\nu$ . The value of  $\gamma$  is  $\gamma = 1.542 \pm 0.005$  using  $\nu = 0.887 \pm 0.009$ .

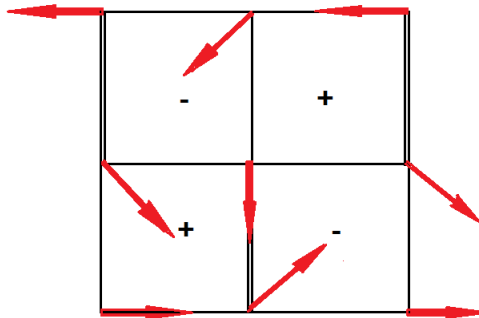


FIG. 26: The square lattice: single (double) bonds are ferromagnetic (antiferromagnetic) bonds. The GS spin configuration is shown by red arrows. The right and left chiralities are denoted by "+" and "-"

at finite  $T$ , the XY spins fluctuate around their GS orientations shown in Fig. 26, making the nature of the phase transition more complex as seen below. Note that some authors have claimed that there are two separate transition of XY and Ising natures [43–46]. However, our results [36] and those of Refs. [41, 42] show clearly that there is only a single transition of the new criticality called "coupled XY-Ising" universality class. We show below our results.

In Ref. [36], using the highly precise multi-histogram MC simulations described above, we have obtained the critical exponents  $\nu$  and  $\gamma$ . We show in Fig. 27 the Binder energy cumulant  $U_E$  [15, 16] as a function of  $L$ : as seen the curve approaches asymptotically  $2/3$  from below. This indicates a second-order nature of the transition.

Let us show the susceptibility versus  $T$  for  $L = 44, 52, 60, 84, 100, 140$  in Fig. 28. A single peak for each size indicates a single transition as observed above. For  $L = 140$  the peak is very close to  $T_c(L = \infty) = 0.45522(2)$  estimated using Eq. (17) and  $\nu = 0.852(2)$  calculated below using the maxima of  $V_1$  and  $V_2$  shown in Fig. 29. The fitting error is less than 0.1%. Note that our value is the same as that of Ref. [42] which used the same multi-histogram MC technique, but differs from those obtained by less efficient methods ( $\nu = 0.816$  in Ref. [45] and  $\nu = 0.889$  in Ref. [46] for XY transition).

We calculate exponent  $\gamma$  using the peak values of  $\chi$  for varying  $L$ . The curve in the  $\ln - \ln$  scale is shown in Fig. 30. The slope gives  $\gamma/\nu$ . Using  $\nu = 0.852$  we obtain  $\gamma = 1.531(3)$  which is different from  $1.448(24)$  obtained by Ref. [45].

At the time of our work in Ref. [36], we did not calculate  $\beta$  and  $\alpha$  as we have done on thin films presented in

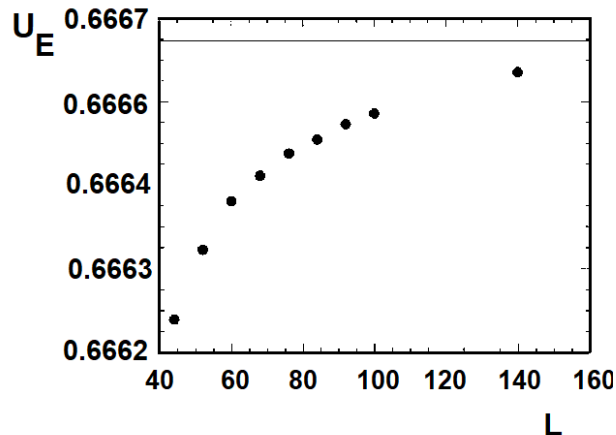


FIG. 27: The Binder energy cumulant  $U_E$  versus  $L$  calculated at  $T_c(L = \infty) = 0.4552(2)$ . The horizontal line indicates  $U_E(L = \infty) = 2/3$ . The results show that the transition is of second order.

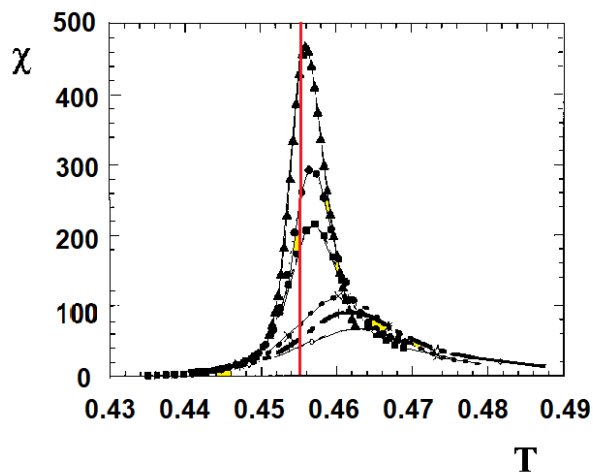


FIG. 28: Susceptibility  $\chi$  versus  $T$  for sizes  $L = 44, 52, 60, 84, 100, 140$  (from lowest to highest curves). The red vertical line is the position of  $T_c(L = \infty)$  calculated with Eq. (TCL) using  $\nu$  obtained by Fig. 29 below.

the preceding section. We were confident on the hyperscalings  $d\nu = \gamma + 2\beta$  and  $\alpha = 2 - d\nu$ , so we used these relations to calculate  $\beta$  and  $\alpha$ . However, in view of the question whether or not these relations are valid in particular cases such as the case of thin films shown in section II and the double transition in the case of fully frustrated square lattice presented here, we would like to check the validity of the hyperscaling relations. We can use  $\nu$  and  $\gamma$  obtained here and the value of  $2\beta/\nu = 0.31(3)$  obtained in Ref. [42], then we have  $d\nu = 2 \times 0.852 = 1.704$  while  $\gamma + 2\beta = 1.531 + 0.31 \times 0.852 = 1.795$ . We see that  $d\nu < \gamma + 2\beta$  even if we take into account errors of the exponents. Note that in these estimations we have used the Rushbrooke "equality" which is so far verified within errors in all known cases.

We note that it has been found in Ref. [42] by direct FSS that  $\alpha/\nu = 0.48(7)$ . Using  $\nu = 0.852$  obtained by us and by Ref. [42], one obtains  $\alpha \simeq 0.409$ . This yields  $2 - \alpha = 2 - 0.409 = 1.591$  which is not equal to  $d\nu = 2 \times 0.852 = 1.704$  (here we do not use the Rushbrooke equality).

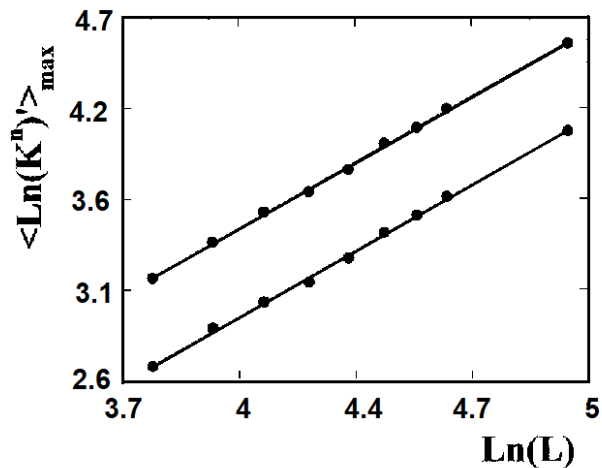


FIG. 29: The maximum of cumulants  $V_1$  and  $V_2$  versus size  $L = 44, 52, 60, 84, 100, 140$  in the  $\ln - \ln$  scale. The slopes give the same  $1/\nu$ . See text for the value of  $\nu$ .

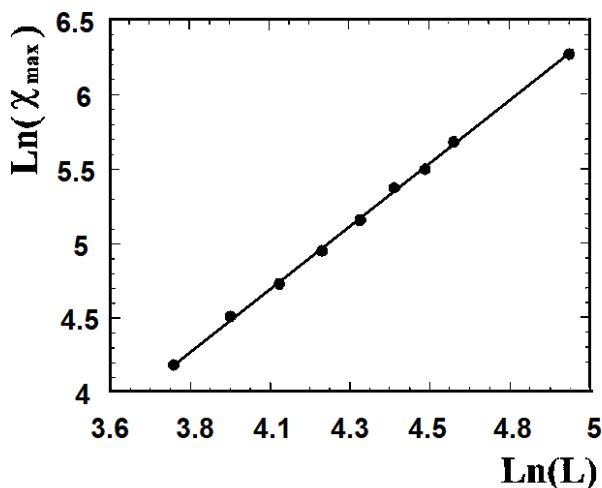


FIG. 30: The maximum of susceptibility  $\chi$  versus size  $L = 44, 52, 60, 84, 100, 140$  in the  $\ln - \ln$  scale. The slope indicates the value of  $\gamma/\nu$ . See text for the value of  $\gamma$ .

The conclusion for this coupled XY-Ising model based on the high-precision multi-histogram technique of our work and of Ref. [42] is that the hyperscaling relation is violated.

### B. Effect of magneto-elastic coupling on criticality

There are certainly other exotic models which may violate the hyperscaling relation for  $d < 4$ . One of these is the magneto-elastic coupling model that we have studied by using the multi-histogram technique [37, 38]. The

$Q$	$\alpha$	$\beta$	$\nu$	$\gamma$	$\eta$
8	0.140(1)	0.310(1)	0.620(5)	1.245(5)	-0.01(1)
5	0.141(5)	0.301(5)	0.620(5)	1.259(5)	-0.03(1)
4	0.135(6)	0.308(5)	0.622(5)	1.249(5)	-0.01(1)
3D Ising	0.1070( <i>a</i> )	0.3265( <i>b</i> )	0.6305( <i>b</i> )	1.2390( <i>b</i> )	0.0370( <i>b</i> )
3	-0.024(4)	0.353(5)	0.675(5)	1.314(5)	0.053(5)
3D XY	-0.0100( <i>a</i> )	0.3455( <i>b</i> )	0.671( <i>b</i> )	1.3150( <i>b</i> )	0.040( <i>b</i> )

TABLE II: Critical exponents obtained by multi-histogram technique for different  $Q$ . *a*: Results from Ref. [47], *b*: Results from Ref. [48]

model consists of atoms on a stacked triangular lattice. Each atom carries an Ising spin and moves around its lattice equilibrium position. There are two kinds of interaction which are distance-dependent: the elastic interaction between atoms and the magnetic interaction between Ising spins. We suppose the following Hamiltonian:

$$\mathcal{H} = U_0 \sum_{i,j} J(r_{ij}) + U_m \sum_{i,j} J(r_{ij}) \sigma_i \dot{\sigma}_j, \quad (23)$$

where the first sum is the elastic interaction with amplitude  $U_0$ , and the second sum expresses the interacting spins with amplitude  $U_m$ . The distance-dependence is supposed to be the Lennard-Jones potential

$$J(r_{ij}) = (r_0/r_{ij})^{12} - 2(r_0/r_{ij})^6, \quad (24)$$

where  $r_0 = 1$  is the distance at equilibrium between NN in the triangular planes and also in the stacking direction.,  $r_{ij} = r_i - r_j$  is the instantaneous distance between NN.

In order to separate the spin disordering from the melting, we take the ratio  $Q = U_0/U_m$  large enough so that the magnetic transition occurs at low  $T$ . The cut-off distance is taken as  $r_c = 1.366r_0$ .

Simulations using multiplex histogram technique have been performed. The reader is referred to Ref. [37, 38] for details. We just summarize the results in Table II. Note that we have calculated at the time of our work (Ref. [37, 38]) only  $\nu$  and  $\gamma$ , and we have relied on the hyperscaling relations  $d\nu = 2 - \alpha$  and  $\gamma/\nu = 2 - \eta$  to calculate  $\alpha$  and  $\eta$  listed in Table II. However, we believe that if  $\alpha$  is directly calculated as in section II, the result of  $\alpha$  may be different, due to the mixing of elastic and magnetic interactions. The nature of the transition depends on  $Q$ : it changes from the Ising nature at large  $Q$  to close to the XY universality class as seen in Table II. In such complex situations, we are not sure that the hyperscaling relations are valid. Further direct calculations of  $\alpha$  in the way we did in Ref. [18] are necessary to conclude on this point.

## VI. CONCLUDING REMARKS

We know that the hyperscaling relation is verified in  $d = 3$  for Ising, XY and Heisenberg spins (results of highly efficient simulations), and in  $d = 2$  for Ising spins (exact results). However, as shown in this review, there are particular cases where the hyperscaling relation  $d\nu = 2 - \alpha$  is violated. One of these situations is the case of a magnetic thin film with small thickness. Another case is the fully frustrated XY square lattice where we show that there is a single phase transition of a new coupled XY-Ising universality: the results of Ref. [42] and our results using the same method of simulation (multiple histogram technique) are the same for  $\nu$  and  $\gamma$ . We did not calculate  $\beta$ , but we believe we should obtain the same  $\beta$  obtained in Ref. [42] in view of the same results obtained for  $\nu$  and  $\gamma$ . The hyperscaling relation is then violated in this case. The case of a system with a magneto-elastic interaction shows a new universality class. The violation, or not, of the hyperscaling relation in this case needs further verifications.

To conclude, let us emphasize that, in view of the precise values we have obtained, at least for thin films, the hyperscaling relation is not verified. We have also presented evidence of the violation of the hyperscaling relation in some other cases. We believe that more cases should be studied before a general conclusion could be drawn. This explains the question mark in the title of this review.

Finally, we note that while revising the present paper, we discover that the hyperscaling relation is also violated in the Kuramoto model with the random case (see [49]).

### Acknowledgments

The authors are grateful to X.-T. Pham-Phu and the late E. H. Boubcheur for participating in some works cited in this paper.

This research received no external funding.

The authors declare no conflict of interest.

- 
- [1] Diep, H. T. Frustrated Spin Systems: Emergence of a Modern Physics, *Comptes Rendus. Physique (France)* **2025** *26*, 225-251.
- [2] Diep, H. T. *Physics of Magnetic Thin Films: Theory and Simulation*, Jenny Stanford Publishing: New York, 2021 (600 pages).
- [3] Diep, H. T. *Theory of Magnetism-Application to Surface Physics*, World Scientific, World Scientific: Singapore, 2014.
- [4] Baxter, R. J. *Exactly Solved Models in Statistical Mechanics*, Academic Press Limited, London (U.K.) 1982.
- [5] Wilson, K. G. Renormalization Group and Critical Phenomena. I. Renormalization Group and the Kadanoff Scaling Picture *Phys. Rev. B* **1971** *4*, 3174.
- [6] Wilson, K. G. Renormalization Group and Critical Phenomena. II. Phase-Space Cell Analysis of Critical Behavior *Phys. Rev. B* **1971** *4*, 3184.
- [7] Fisher, M.E. The theory of critical point singularities. In *Critical Phenomena, Proceedings of the 51st Enrico Fermi Summer School, Varenna*; Green, M.S., Ed.; Academic Press: New York, NY, USA, **1971**; p. 1.
- [8] Fisher, M.E.; Barber, M.N. Scaling theory for finite-size effects in the critical region *Phys. Rev. Lett.* **1972**, *28*, 1516.
- [9] Cardy, J. *Scaling and renormalization in statistical physics*, Cambridge University Press: Cambridge (U.K.), 1996.
- [10] Berche, B.; Ellis, T.; Holovatch, Y.; Kenna, R. Phase transitions above the upper critical dimension *SciPost Phys. Lect. Notes* **2022**, *60*, 1.
- [11] Young, A. P. Violations of Hyperscaling in Finite-Size Scaling above the Upper Critical Dimension, *Entropy* **2024** *26(6)*, 509; <https://doi.org/10.3390/e26060509>.
- [12] Honchar, Yu.; Berche, B.; Holovatch, Yu.; Kenna, R. When correlations exceed system size: finite-size scaling in free boundary conditions above the upper critical dimension, *Condensed Matter Physics* **2024**, *27*, 13603:1-15.
- [13] Luijten, E. and Blöte, H.W.J. Finite-Size Scaling and Universality above the Upper Critical Dimensionality, *Phys. Rev. Lett.* **1996**, *76*, 1557.
- [14] O'Connor, D.; Stephens, C.R. ; Bray, A.J. Dimensional crossover in the large-N limit. *J. Stat. Phys.* **1997**, *87*, 273-291.
- [15] Ferrenberg, A. M. ; Swendsen, R. H. New Monte Carlo technique for studying phase transitions, *Phys. Rev. Lett.* **1988** *61*, 2635. Erratum *Phys. Rev. Lett.* **1989** *63*, 1658.
- [16] Ferrenberg, A. M.; Swendsen, R. H. Optimized Monte Carlo data analysis, *Phys. Rev. Lett.* **1989** *63*, 1195 .
- [17] A. Bunker, A.; Gaulin, B. D.; Kallin, C. Multiple-histogram Monte Carlo study of the Ising antiferromagnet on a stacked triangular lattice, *Phys. Rev. B* **1993** *48*, 15861-15872.
- [18] Pham-Phu, X.-T.; Ngo, V.-Thanh; Diep, H. T. Critical behavior of magnetic thin films, *Surface Science* **2009** *603*, 109–116.
- [19] Capehart, T. W.; Fisher, M. E. Susceptibility scaling functions for ferromagnetic Ising thin films, *Phys. Rev. B* **1976** *13*, 5021-5038.
- [20] Binder, K. The Monte Carlo Method for the Study of Phase Transitions: A Review of Some Recent Progress, *J. of Computational Physics* **1985** *59*, pp. 1-55.
- [21] Ferrenberg, A.M.; Landau, D.P. Critical behavior of the three-dimensional Ising model: A high-resolution Monte Carlo study, *Phys. Rev. B* **1991** *44*, 5081-5091.
- [22] Diep, H. T.; Levy, J.C.S.; Nagai, O. Effects of Surface Spin Waves and Surface Anisotropy in Magnetic Thin Films at Finite Temperatures, *Phys. Stat. Solidi (b)* **1979** *93*, 351-361.
- [23] Diep, H.T. Temperature-Dependent Surface Magnetization and Critical Temperature of Ferromagnetic Thin Films, *Phys. Stat. Solidi (b)* **1981**, *103*, 809-815.
- [24] Diep, H. T. Quantum theory of helimagnetic thin films, *Phys. Rev. B* **2015** *91*, 014436 (12 pp.).
- [25] El Hog, S.; Diep, H. T.; Puzzkarski, H. Theory of magnons in spin systems with Dzyaloshinskii–Moriya interaction, *J. Phys.: Condens. Matter* **2017** *29* 305001 (10pp.).
- [26] Sharafullin, I.; Kharrasov, M. Kh.; Diep, H. T. Dzyaloshinskii-Moriya interaction in magnetoferroelectric superlattices: Spin waves and skyrmions, *Phys. Rev. B* **2019** *99*, 214420 (14 pp.).
- [27] Schilbe, P.; Siebentritt, S.; and Rieder, K. H. Monte Carlo calculations on the dimensional crossover of thin Ising films *Phys. Lett. A* **1996** *216*, 20-25.
- [28] Pham-Phu, X. T.; Ngo, V. T.; Diep, H. T. Cross-Over from First- to Second-Order Transition in Frustrated Ising Antiferromagnetic Films, *Phys. Rev. E* **2009** *79*, 061106 (8 pp.).
- [29] Wang, F.; Landau, D.P. Efficient, Multiple-Range Random Walk Algorithm to Calculate the Density of States, *Phys. Rev. Lett.* **2001** *86*, 2050-2053.
- [30] Brown, G.; Schulhess, T. C. Wang–Landau estimation of magnetic properties for the Heisenberg model, *J. Appl. Phys.* **2005** *97*, 10E303.

- [31] B. J. Schulz, B. J.; Binder, K.; Müller, M.; Landau, D.P. Avoiding boundary effects in Wang-Landau sampling, *Phys. Rev. E* **2003** *67*, 067102 (2 pp.).
- [32] Malakis, A.; Martinos, S.S.; Hadjiagapiou, I.A.; Fytas, N.G.; Kalozoumis, P. Entropic sampling via Wang-Landau random walks in dominant energy subspaces, *Phys. Rev. E* **2005** *72*, 066120 (11 pp.).
- [33] Ngo, V. T.; Diep, H.T., Phase Transition in Heisenberg Stacked Triangular Antiferromagnets: End of a Controversy, *Phys. Rev. E* **2008** *78*, 031119.
- [34] Ngo, V.T.; Diep, H. T. Stacked Triangular XY Antiferromagnets: End of a Controversial Issue on the Phase Transition, *J. Appl. Phys.* **2008** *103*, 07C712.
- [35] Ngo, V.T. ; Hoang, D.-Tien; Diep, H. T. First-Order Transition in XY Fully Frustrated Simple Cubic Lattice, *Phys. Rev. E* **2010** *82*, 041123 (5 pages).
- [36] Boubcheur, E. H.; Diep , H. T. Critical behavior of the two-dimensional fully frustrated XY model, *Phys. Rev. B* **1998** *58*, 5163-5165.
- [37] Boubcheur, E. H.; Diep, H. T. Effect of elastic interaction on critical behavior of three-dimensional Ising model, *J. Appl. Physics* **1999** *85*, 6085-6087.
- [38] Boubcheur, E. H.; Massimino, P.; Diep, H. T. Effects of magnetoelastic coupling: critical behavior and structure deformation, *Journal of Magnetism and Magnetic Materials* **2001** *223*, 163-168.
- [39] Berge, B.; Diep , H. T. ; Ghazali, A.; Lallemand, P. Phase transitions in two-dimensional uniformly frustrated XY spin systems, *Phys. Rev. B* **1986** *34*, 3177-3184.
- [40] Granato, E.; Nightingale, M. P. Chiral exponents of the square-lattice frustrated XY model: a Monte Carlo transfer-matrix calculation, *Phys. Rev. B* **1993** *48*, 7438-7444.
- [41] Lee, J.; Kosterlitz, J. M.; Granato, E. Monte Carlo study of frustrated XY models on a triangular and square lattice, *Phys. Rev. B* **1991** *43*, 11531-11534.
- [42] Granato, E.; Kosterlitz, J.M.; Lee, J.; Nightingale, M. P. Phase transitions in coupled XY-Ising systems, *Phys. Rev. Lett.* **1991** *66*, 1090-1093.
- [43] Olsson, P. Two Phase Transitions in the Fully Frustrated XY Model, *Phys. Rev. Lett.* **1995** *75*, 2758-2761.
- [44] Jeon, G. S.; Park, S. Y.; Choi, M. Y. Double transitions in the fully frustrated XY model, *Phys. Rev. B* **1997** *55* 14088-14091.
- [45] Lee, S. ; Lee, K.C. Phase transitions in the fully frustrated XY model studied with use of the microcanonical Monte Carlo technique, *Phys. Rev. B* **1994** *49*, 15184-15189.
- [46] Ramirez-Santiago, G; Jose, J. V. Critical exponents of the fully frustrated two-dimensional XY model, *Phys. Rev. B* **1994** *49*, 9567-9582.
- [47] Antonenko, S. A.; Sokolov, A. I. Critical exponents for a three-dimensional  $O(n)$ -symmetric model with  $n > 3$ , *Phys. Rev. E* **1995** *51*, 1894-1898.
- [48] Le Guillou, J. C.; Zinn-Justin, J. Accurate critical exponents from the  $\epsilon$ -expansion, *J. Phys. (France) Lett.* **1985** *46*, L137-141.
- [49] Hong, H.; Chaté H.; Tang, L. ; Park, H. Finite-size scaling, dynamic fluctuations, and hyperscaling relation in the Kuramoto model, *Physical Review E* **2015** *92*(2).